

# Simulation of soil erosion under the influence of climate change scenarios

Mohammad Zare<sup>1</sup> · Ali Akbar Nazari Samani<sup>1</sup> · Majid Mohammady<sup>2</sup> · Teimur Teimurian<sup>3</sup> · Javad Bazrafshan<sup>4</sup>

Received: 1 February 2016 / Accepted: 8 October 2016 / Published online: 27 October 2016  
© Springer-Verlag Berlin Heidelberg 2016

**Abstract** Climate change is known as the long-term average changes of weather conditions in an area with significant effects on the ecosystem of the region. Climate change is believed to have significant impacts on the water basin and region, such as in a runoff and hydrological system, erosion, environment as well as agriculture. Climate change simulation and scenario design can serve as a useful tool in reducing the effects of this phenomenon. The objective of this study is to simulate climate change and design different scenarios in order to evaluate the site-specific impacts of future climate change on soil erosion at the Kasilian watershed in the north of Iran employing seven downscaling scenarios. Hence, the climate changes were downscaled based on A2 and B1

emission scenarios, using the Institut Pierre Simon Laplace (IPCM4) with Long Ashton Research Station Weather Generator model and three climate change scenarios, i.e., 10% increase in rainfall, 10% reduction in rainfall and unchanged rainfall were employed by Statistical Downscaling Model for the periods of 2011–2030 and 2031–2050. Also, the Revised Universal Soil Loss Equation (RUSLE) model was used in order to estimate soil erosion in basis period (1991–2010) and in the simulated periods (2011–2030, 2031–2050) under effect of climate change scenarios. The results showed that the rainfall erosivity factor in the RUSLE model is directly influenced by climate changes. The mean of soil erosion was 21.82 (tons ha<sup>-1</sup> year<sup>-1</sup>) in basis period, and there was an increase of 10–35% for rainfall erosivity and 10–32% for soil loss during 2011–2030, compared with the present climate. Simulated soil loss under the rainfall erosivity during 2031–2050 would be 4–28 and 2–26% for soil loss compared with those under seven downscaling scenarios in the present climate. Thus, increase in soil erosion will be definite in four future decades.

✉ Majid Mohammady  
majid.mohammady@semnan.ac.ir

Mohammad Zare  
mzare91@ut.ac.ir

Ali Akbar Nazari Samani  
aknazari@ut.ac.ir

Teimur Teimurian  
t.teimurian@ut.ac.ir

Javad Bazrafshan  
jbazr@ut.ac.ir

**Keywords** Rainfall erosivity · SDSM · LARS-WG · RUSLE · Iran

## Introduction

Globally, soil erosion is one of the most significant forms of soil degradation (Portenga and Bierman 2011; Alkharabsheh et al. 2013) due to the fact that adverse influences of widespread soil erosion on soil degradation, agricultural production, water quality, hydrological systems and environments have long been recognized as severe problems for human sustainability (Lal 1998). Soil

<sup>1</sup> Faculty of Natural Resources, University of Tehran, Tehran, Iran

<sup>2</sup> Department of Range and Watershed Management Engineering, College of Natural Resources, Semnan University, Semnan, Iran

<sup>3</sup> Department of Watershed Management Engineering, Faculty of Natural Resources, University of Tehran, Tehran, Iran

<sup>4</sup> Department of Irrigation and Reclamation Engineering, University of Tehran, Tehran, Iran

erosion can be evaluated from two issues, including: on-site and off-site issues. On-site issues include a reduction in the water and nutrient-holding capacity of soils, loss of organic matter and a reduction in soil depth to support roots and biota (Wardle et al. 2004; Pimentel 2006; Mullan 2013). The off-site issues are often more evident and include loading and sedimentation of watercourses and reservoirs and increases instream turbidity, all of which can disturb aquatic ecosystems and upset the geomorphological functioning of river systems (Shiono et al. 2013). Erosion brings about deterioration of soil structure which decreases the infiltration rate, thereby increasing runoff. This implies that less water is available for plants (Pimentel 2006). In the long-term, top soil can get lost; hence, fertility and productivity could decrease (Lal 2001). Soil erosion is influenced by several factors such as climate, land use and topography with climate as one of the major factors of soil erosion. Climate change is believed to have significant impacts on the water basin and region, such as in a runoff and hydrological system, erosion, environment and agriculture. Soil erosion also responds to the total amount of rainfall along with the differences in rainfall intensity; however, the dominant variable appears to be rainfall intensity and energy rather than rainfall amount alone. One study has predicted that for every 1% increase in total rainfall, erosion rate would increase only by 0.85% if there was no correspondent increase in rainfall intensity. On the other hand, if both amount and intensity of rainfall were to change simultaneously, it is predicted in a statistically representative manner that erosion rate will increase by 1.7% for every 1% increase in total rainfall (Pruski and Nearing 2002a). Precipitation change in the form of intensity and amount of rainfall is one of the most direct influences on runoff and soil erosion (Nearing et al. 2005; Pruski and Nearing 2002b). Some studies have shown that the rate of soil erosion quickly responds to any change in rainfall such as intensity, duration and frequency of rainfall or the rainfall seasonal patterns (Meusburger et al. 2012; Serpa et al. 2015; Simonneaux et al. 2015). Climate change leads to changes in climate variables such as precipitation, temperatures, wind and solar radiation that these changes affect soil erosion (Shiono et al. 2013). The most direct of the impacts of climate change on soil erosion is the change in rainfall erosivity (Favis-Mortlock and Guerra 1999; Mullan et al. 2012). Atmospheric-Ocean General Circulation Models (GCMs) is a major source of global climate for present and future simulations using different scenarios of climate change (IPCC 2001). Downscaling techniques are employed to convert the coarse spatial resolution of the GCMs output into a fine resolution. There are various downscaling techniques for investigating future climate change and estimation of climate parameters such as precipitation, temperature. Dibike and Coulibaly (2005) and

Hassan et al. (2014) compared LARS-WG<sup>1</sup> and SDSM<sup>2</sup> downscaling techniques with results showing that the SDSM has a better performance when compared to LARS-WG; however, SDSM is slightly underestimated for the wet- and dry-spell lengths. Furthermore, findings of Dibike and Coulibaly (2005) for maximum and minimum temperatures illustrated that SDSM provides a slightly better result when compared to LARS-WG. In the research of Liu et al. (2011), SDSM and bilinear interpolation (delta) methods were utilized to generate daily series in the Yellow River Basin. The results showed that SDSM is more accurate for downscaling of climate parameters. Researcher also explained that SDSM is not a suitable method for estimating the daily precipitation series (Chu et al. 2008; Hessami et al. 2008; Liu et al. 2008). Nearing (2001), Pruski and Nearing (2002a, b), Plangoen and Babel (2014) applied the delta change method to generate future precipitation, and results showed that this model has enough accuracy as a downscaling technique.

A numbers of studies have reported the potential impact of climate change on soil erosion (Imeson and Lavee 1998; Oneal et al. 2005; Bosco et al. 2009; Zhang et al. 2009; Maeda et al. 2010; Mullan et al. 2012; Mullan 2013; Shiono et al. 2013; Litschert et al. 2014). Given the potential of climate change to increase soil erosion and its associated adverse impacts, modeling future rates of erosion is a fundamental step in its assessment as a potential future environmental problem. Prediction models have become increasingly important tools in assessing soil erosion and are the only practicable means in assessing the response of soil erosion to future climate change (Lal 1998). To provide an effective result for soil erosion hazard assessment and simulation of soil erosion risk in future, remote sensing (RS) and geographical information system (GIS) technologies were adopted and a numerical model was developed using RUSLE<sup>3</sup> method. In the following, we computed soil loss for a basis period (1991–2010) and for two future time periods (2011–2030 and 2031–2050) for each of four sets of down-scaled climate data corresponding to two Intergovernmental Panel on Climate Change (IPCC) global emissions scenarios (A2, B1) each modeled using one GCMs (HadCM3).

## Materials and methods

### Study area

Kasilian watershed is the section of Tallar catchment which is located in the central region of north Iran. Surface area of

<sup>1</sup> Long Ashton Research Station Weather Generator.

<sup>2</sup> Statistical Downscaling Model.

<sup>3</sup> Revised Universal Soil Loss Equation.

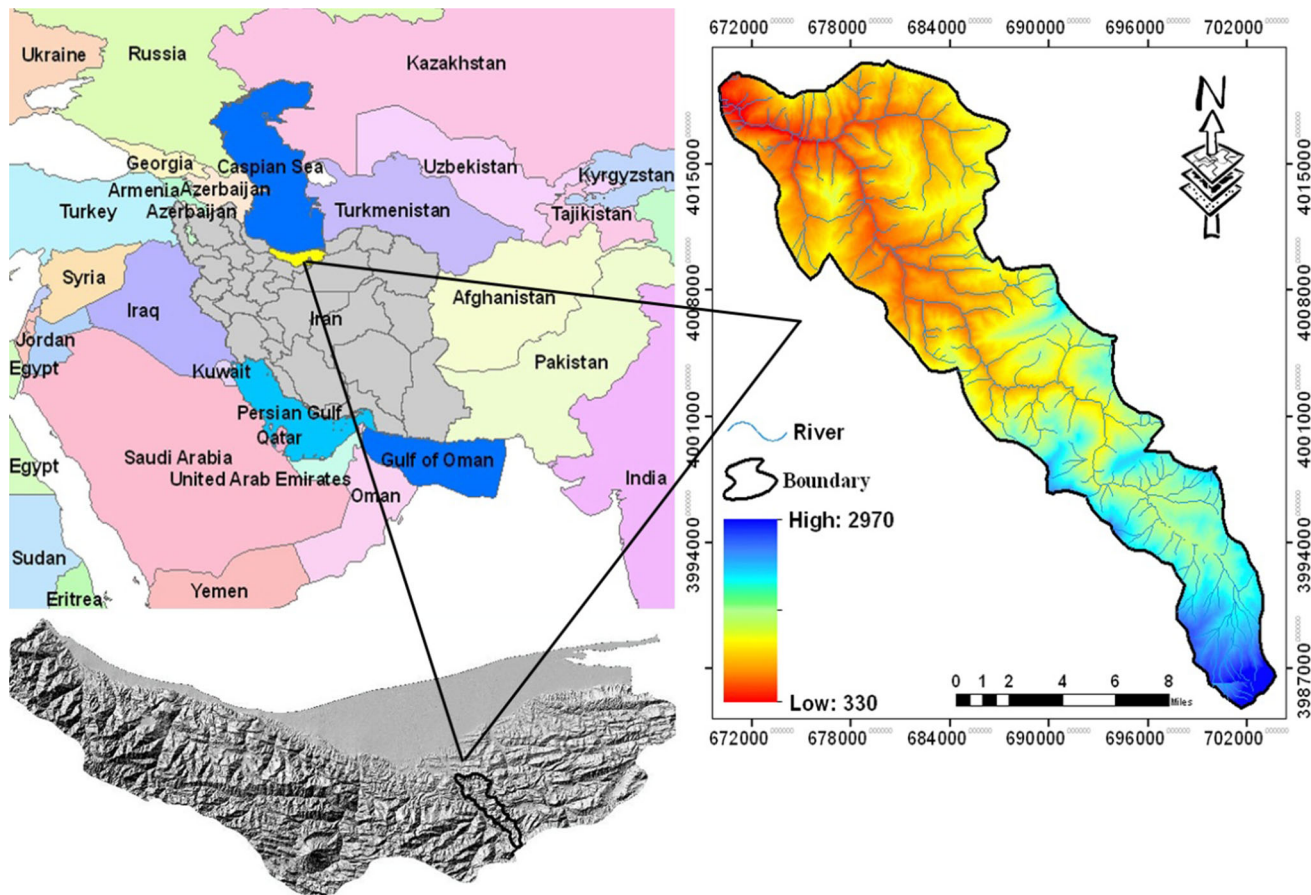


**Fig. 1** Location of Kasilian watershed

the watershed is 342.86 km<sup>2</sup>, and its coordinates are 53°1′–53°26′E and 35°1′–36°32′N (Fig. 1). The minimum and maximum heights of the watershed are 286 and 3288.88 m above sea level, respectively, and its average precipitation equals 733.3 mm in semi-humid and cold climate. In terms of Iranian geological classification, this watershed belongs to central Alborz with its surface rocks belonging to the first, second and third eras. The majority of this watershed is covered with different forest species containing other land uses such as farm, rural and agricultural uses. Its soil is primarily of podzolic, brown forest and sedimentary types. In recent years, a lot of rangeland and agricultural lands were converted into residential areas due to favorable climatic conditions.

**Methods**

In this study, future climate change scenarios were simulated in order to evaluate their potential impacts on soil erosion in Kasilian, Iran. To achieve this objective, data were provided from rain gauge stations of Kasilian watershed as well as calculating the rainfall erosivity index in the basis period (1991–2010), and then the daily rainfall

data inputted into LARS-WG model along with the rainfall data of two future periods (2011–2030, 2031–2050) were generated based on A2 and B1 scenarios. In the next step, based on the generated data, the rainfall erosivity index of the next period is provided, and the zoning map of rainfall erosivity in the basis and future periods was obtained and compared. In this study, RUSLE model was employed to estimate the average annual soil loss (Renard et al. 1997) using ArcGIS 10.3. The following sections illustrate the computation of the *R*, *K*, *LS*, *C* and *P* factors from precipitation data, soil surveys, a digital elevation model (DEM) and land use maps. The spatial resolution of the data was set at 30 m, which is consistent with the Landsat thematic image. A flowchart describing the components of the modeling framework is presented in Fig. 2, while the main components involved in the study are shown in detail below.

**Downscaling**

GCMs provide physically-based predictions of the way climate might change as a result of increasing concentrations of atmospheric CO<sub>2</sub> and other trace gases. However,

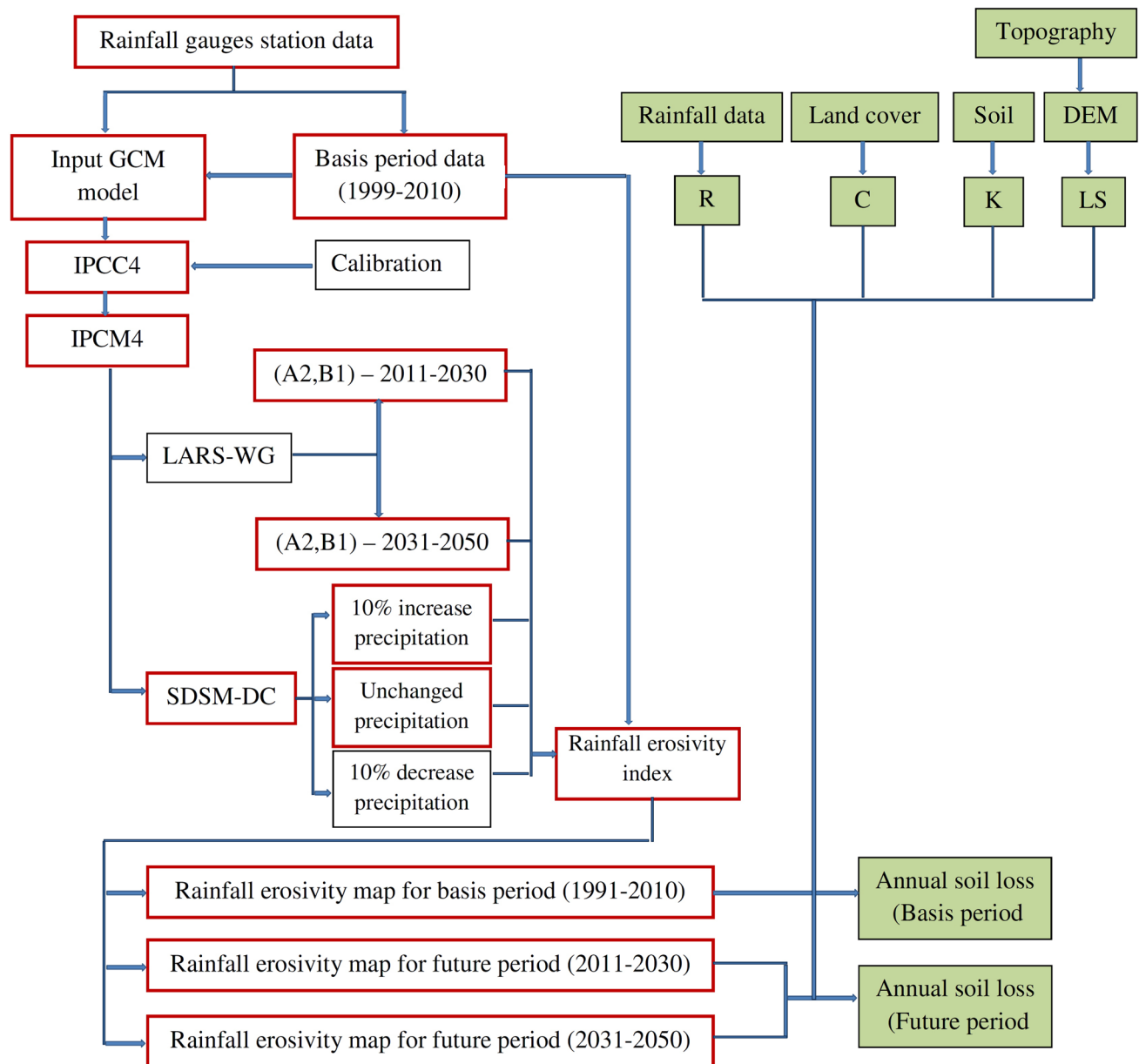


**Fig. 2** Research flowchart

they were not designed for climate change impact studies and do not provide a direct estimation of hydrological response to climate change (Liu et al. 2011). The GCM outputs need to be converted into a reliable daily rainfall series at the selected watershed scale (Dibike and Coulibaly 2005). So-called downscaling techniques are usually used to estimate local and regional climate information extracted from atmospheric large data or output of global circulation models (Wilby et al. 2002). Statistical downscaling relies on developing mathematical transfer functions between observed large-scale predictor variables and the surface environmental variable of interest (local-scale predictands) for the present day and in a subsequent forcing

of these transfer functions for the future under the guidance of general circulation models (Wilby et al. 2002). SDSM-DC and LARS-WG methods are used to generate daily series.

### Statistical Downscaling Model (SDSM)

SDSM is a decision support tool for assessing local climate change impacts using a robust statistical downscaling technique. The SDSM uses a conditional process to downscale precipitation. Local precipitation amounts depend on wet-/dry-day occurrences, which in turn depend on regional-scale predictors (Wilby et al.

2002). SDSM is best described as a hybrid of the stochastic weather generator and regression-based methods. It mainly contains four parts: (1) identification of predictions and predictors; (2) model calibration; (3) weather generator; and (4) generation of future series of climate variables (Liu et al. 2011).

**LARS-WG**

LARS-WG model is one of the most famous random data generating models used for simulation of the rainfall amounts, minimum and maximum temperatures and solar radiation in a single location under the present and future climate conditions (Semenov et al. 2010). This model is consisted of three parts including calibration, evaluation and generation or simulation of meteorological data of the coming decades. The basic requirement of model in calibration step is a file that specifies the behavior of the climate in the previous period. This file is prepared using the daily data of climatic parameters in the study region obtained from Water Resources Management Organization in Mazandaran Province by considering a basis period to perform the model.

**Climate change scenarios**

The rainfall data were obtained from 1991 to 2010 (basis period) and inputted into the model, and then data evaluation and generation of meteorological data were implemented for two statistical periods of 2011–2030 and 2031–2050 (future period). After ensuring the accuracy of six weather stations’ rainfall data and examining their homogeneity using Pettit and SNHT<sup>4</sup> test in the XLSTAT software at probability level 95%, data were converted into the related format while the LARS-WG and SDSM models were calibrated for this period. To investigate the accuracy of the calibrated model, the root-mean-square error (RMSE) and mean difference (BIAS) were used as shown in the following equation:

$$RMSE = \sqrt{\frac{1}{n} \sum (X_i - Y_i)^2} \tag{1}$$

$$BIAS = \frac{\sum_{i=1}^n (X_i - Y_i)}{n} \tag{2}$$

where  $X_i$  and  $Y_i$  are the values observed and estimated by the model for each station and  $n$  is the total number of evaluated samples (Hassan et al. 2014). After ensuring the capability of LARS-WG and SDSM model in the proper simulation of rainfall amounts in the basis period, this model was simulated for statistical downscaling the IPCM4

global circulation model data to simulate the rainfall during the next period to generate synthetic data over the next two periods in each of the stations.

In the scenario making using SDSM model, the series of observed daily weather and NCEP<sup>5</sup> data set were employed, and by utilizing large-scale atmospheric variables extracted from GCM model, simulated climate scenarios were produced for present and future periods (Wilby and Harris 2006). In this part of the study, three scenarios, i.e., 10% increase in precipitation, 10% reduction in precipitation and unchanged precipitation for future, were used.

**RUSLE model**

The RUSLE is an empirical erosion model designed to predict long-time average annual soil loss by runoff (Park et al. 2011; Pradeep et al. 2015). The RUSLE represents how climate, soil, topography and land use affect rill and interrill soil erosion caused by raindrop impact and surface runoff (Renard et al. 1997). Therefore, this paper uses the RUSLE empirical model to predict annual loss. The RUSLE can be expressed as (Renard et al. 1997)

$$A = R \times K \times L \times S \times C \times P \tag{3}$$

where  $A$  is the average soil loss caused by erosion (tons ha<sup>-1</sup> year<sup>-1</sup>),  $R$  is the rainfall erosivity factor,  $K$  is the soil erodibility factor,  $L$  is the slope length factor,  $S$  is the slope steepness factor,  $C$  is the cover and management practice factor, and  $P$  is the conservation support practice factor.

**Calculation of RUSLE parameters**

*Rainfall erosivity factor (R)*

The rainfall factor is a numerical descriptor of the ability of rainfall to erode soil (Vrieling et al. 2014; Nearing et al. 2015).  $R$  factor in RUSLE model is considered as rainfall erosivity index and defined based on maximum rainfall intensity, and this factor is calculated with two parameters of total rainfall kinetic energy with 30-min maximum rainfall (Eq. 4):

$$R = \frac{1}{n} \sum_{i=1}^n \left[ \sum_{k=1}^m KE(I_{30}) \right] \tag{4}$$

where  $R$  is rainfall erosivity (MJ mm ha<sup>-1</sup> h<sup>-1</sup> year<sup>-1</sup>),  $KE$  is the total kinetic energy of each shower (MJ ha<sup>-1</sup>),  $I_{30}$  is the maximum intensity of 30-min rainfall (mm h<sup>-1</sup>) (Renard and Freimund 1994). Also, the kinetic energy of each shower is calculated through Wischmeier and Smith equation (1978) (Eq. 5):

$$KE = (11.98 + 8.73 \log_{10} I) \tag{5}$$

<sup>4</sup> Standard Normal Homogeneity Test.

<sup>5</sup> National Centers for Environmental Prediction.

There were only a limited number of rainfall register stations in Kasilian watershed and its surrounding which makes the calculation of rainfall erosivity difficult. Therefore, in order to overcome this defect, the monthly and annual average rainfall amounts were employed to estimate *R* factor by Renard and Freimund (1994) equation resulting from Wischmeier studies. Hence, after determining the desired stations, the monthly and annual rainfall was achieved. In the next step, Fournier index and *R* factor obtained for all rain gauge stations in Kasilian watershed using Eq. 6.

$$F = \frac{\sum_{i=1}^{12} P_i^2}{\sum_{i=1}^{12} P} \tag{6}$$

where *P<sub>i</sub>* is the average rainfall (mm) and *p* is the annual average rainfall (mm).

Fournier index equation was calculated for stations with rain gauge. In the next step, there was a relationship between the values obtained from Fournier index and rainfall erosivity index. There was also a similar relationship between rainfall erosivity index values with 24-h rainfall and the annual rainfall values, and finally among Fournier index, 24-h rainfall and the annual rainfall the best factor that was able to make a relationship with rainfall erosivity index was fitted on the other stations without rain gauge. Finally, the rainfall erosivity map in Kasilian watershed was prepared using the interpolation method in ArcGIS 10.3 software.

*Soil erodibility factor (K)*

The soil erodibility factor (*K*) describes the susceptibility of soil to erosion by rainfall (Ward et al. 2009). The *K* factor is related to soil texture, organic matter content, permeability and other factors and is basically derived from the soil type (Wischmeier et al. 1971). In this study, *K* factor was calculated using equation that requires four steps of calculation (Auerswald et al. 2014):

1.  $K_1 = 2.77 \times 10^{-5} \times (f_{si+vfSa} \times (100 - f_{cl}))^{1.14}$   
for  $f_{si+vfSa} < 70 \%$
- $K_1 = 1.77 \times 10^{-5} \times (f_{si+vfSa} \times (100 - f_{cl}))^{1.14}$   
 $+ 0.0024 \times f_{si+vfSa} + 0.16$  for  $f_{si+vfSa} > 70 \%$

**Table 1** Evaluation in rainfall simulation of basis period

Station	MBE	RMSE	R <sup>2</sup>
Darzi Kola	3.06	3.86	0.9643
Kaleh	4.22	6.55	0.9395
Rig Cheshmeh	9.3	11.3	0.8945
Sangdeh	3.89	5.97	0.9609
Shirgah	8.83	10.54	0.9127
Talar	6.73	7.51	0.9254

2.  $K_2 = (12 - f_{OM})/10$  for  $f_{OM} < 4 \%$   
 $K_2 = 0.8$  for  $f_{OM} > 4 \%$
3.  $K_3 = K_1 \times K_2 + 0.043 \times (A - 2) + 0.033 \times (P - 3)$   
for  $K_1 \times K_2 > 0.2$   
 $K_3 = 0.091 - 0.34 \times K_1 \times K_2 + 1.79 \times (K_1 \times K_2)^2$   
 $+ 0.24 \times K_1 \times K_2 \times A + 0.033 \times (P - 3)$   
for  $K_1 \times K_2 < 0.2$
4.  $K = K_3$  for  $f_{rf} < 1.5 \%$   
 $K = K_3 \times (1.1 \times \exp(-0.024 \times f_{rf}) - 0.06)$   
for  $f_{rf} > 1.5 \%$  (7)

where *f<sub>si+vfSa</sub>*: mass fraction (in%) of silt plus very fine sand Si + vfSa (2...100 μm) in the fine earth fraction, *f<sub>cl</sub>*: mass fraction (in%) of clay (<2 μm) in the fine earth fraction, *f<sub>OM</sub>*: mass fraction (in%) of organic matter in the fine earth fraction, A: soil structure index (1...4) increasing from very fine granular to blocky, platy or massive (for definition of the classes, see Wischmeier et al. 1971), C: permeability index (1...6) increasing from rapid to very slow (for definition of the classes, see Wischmeier et al. 1971).

*Slope length and steepness factor (LS)*

The slope length factor *L* is defined as the distance from the source of runoff to the point where deposition begins, or runoff becomes focused into a defined channel. As slope length increases, the overland flow and flow velocity also increase steadily, resulting in greater erosion forces applied to the soil surface (Ranzi et al. 2012). The equation of Moore and Burch (1986), adopted for estimates of erosion at the catchment scale, was used.

$$L = 1.4[A_s/22.13]^{0.4} \tag{8}$$

$$S = [\text{Sin}\beta/0.0896]^{1.3} \tag{9}$$

where *A<sub>s</sub>* is the area of plot per unit width and β is slope angle, computed from the DEM.

*P factor (erosion control practice factor)*

*P* factor is the ratio of soil loss with a specific support practice to the corresponding loss with upslope and downslope cultivation (Renard et al. 1997). As there is no significant support practice for land in Iran (and information on subsurface drainage is not available), this factor is assumed to be equal to 1 for Kasilian watersheds.

*Cover management factor (C factor)*

The land cover and management factor represent the effects of vegetation, management and erosion control

practices on soil loss (Renard et al. 1997). The *C* factor expresses the relation between erosion on bare soil and erosion under cultivation and is based on plant cover, production level and cropping techniques.

### Simulation of soil erosion

After preparing the required factors for RUSLE model, they were entered into ArcGIS 10.3 software and were multiplied in Raster calculator. In order to simulate erosion values, *K*, *C*, *LS* and *P* factors were assumed to be constant for simulation period. In addition, to estimate rainfall erosivity by the use of LARS-WG downscaling model and two scenarios A2 and B1, precipitation values for the periods of 2011–2030 and 2031–2050 were produced. Employing SDSM-DC model, three scenarios were applied and precipitation values for all three scenarios of the model for the years 2011–2030 and 2031–2050 were prepared. Subsequently, each of these values was inserted into RUSLE model after being converted into rainfall erosivity values.

## Results and discussion

### Calibration and validation of SDSM and LARS-WG

Results of LARS-WG model accuracy assessment in rainfall simulation are shown in Table 1. According to this table, the accuracy evaluation was assessed based on  $R^2$ , RMSE and BIAS indices for a 20-year period from 1991 to 2010 in six stations. Results indicated that there was an agreement between the simulated and observed amounts while low amounts of RMSE and BIAS and high amount of  $R^2$  in different stations showed the same agreement. These results indicate that LARS-WG model has reasonable power in downscaling the rainfall data in IPCC4 model.

For illustrative purposes, the comparisons of monthly mean of the simulated and observed rainfall are shown in Fig. 3 for the study area. There are good matches between monthly mean of the simulated and observed precipitation. So, the mentioned model can be employed to generate the climatic data over the anticipated period. Ashraf et al. (2010) also emphasized the appropriate ability of IPCC4 model in small scaling of rainfall data in Iran. Dibike and Coulibaly (2005), Hashmi et al. (2009) and Hassan et al. (2014) also showed daily rainfall was well simulated by the LARS-WG method. SDSM enables the production of climate change time series at sites, for which there are daily data for model calibration, as well as archived GCM output to generate scenarios for future decades. The recent Decision Centric (SDSM-DC)

version can also produce synthetic weather series and fill gaps in observed meteorological data (Wilby et al. 2014). The parameters established during the calibration process between observation and simulation data were utilized for validation. The mean daily precipitation, average wet- and dry-spell lengths were employed as statistical performance evaluation criteria. Furthermore, Fig. 4 shows comparison of the downscaled and observation precipitation during the validation period for Sangdeh station. Results showed that the SDSM model is a useful tool for generating daily weather data under different scenarios, based on expert's opinions in present and future periods. Dibike and Coulibaly (2005), Khan et al. (2006), Xu et al. (2009) and Hassan et al. (2014) also confirmed that SDSM is a suitable model to precipitation downscaling. Generally, these models have shown enough accuracy in several researches as expected Hassan et al. (2014), and Dibike and Coulibaly (2005) explained that SDSM underestimates for the wet- and dry-spell lengths throughout the year. Therefore, SDSM and LARS-WG are suitable methods for estimating the mean daily precipitation and wet-/dry-spell length, respectively. As earlier mentioned, there are various downscaling techniques available; however, the one that provides the most reliable estimates of daily rainfall time series was not clearly stated (Dibike and Coulibaly 2005).

### Climate change scenarios

Regional changes in annual average rainfall in different stations of LARS-WG scenarios are shown in Table 2. As shown in the table, the maximum rainfall in the basis period is related to the Shirgah station (1045 mm) while the minimum rainfall is for Darzi Kola station (618 mm). The comparison of mean rainfall in the basis period and simulated period at difference stations shows in all scenarios the amount of rainfall was more than that of the basis period. The results show the amount of rainfall will increase 12% in A2 scenario and 14% in B1 scenario in comparison to the basis period by the year 2030. The results also indicate that there will be 4 and 7% increase in rainfall in A2 and B1 scenario, respectively, by the year 2050 when compared to the basis period. Liu et al. (2011), Plangoen and Babel (2014) also explained continued increase in precipitation during the twenty-first century. In order to investigate the role of different months of the year in the amount of rainfall erosivity and its effect on erosion, different months in two simulated periods and basis period were compared using the mean of monthly rainfall in the observed and simulated periods under A2 and B1 scenarios of LARS-WG model (Fig. 5). The results showed that the mean of monthly rainfall in both scenarios was more than

**Fig. 3** Comparison of the observed and simulated mean monthly precipitation using LARS-WG in the basis period (1991–2010)

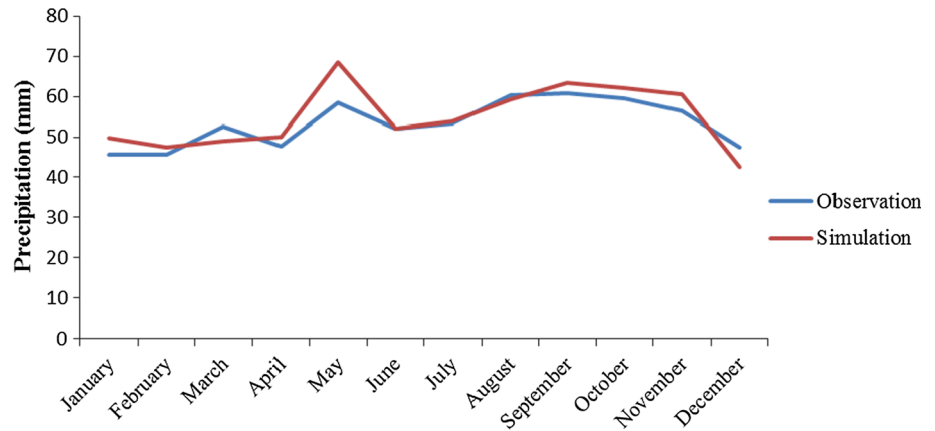


**Fig. 4** Validation results of SDSM downscaling for precipitation for Sangdeh station

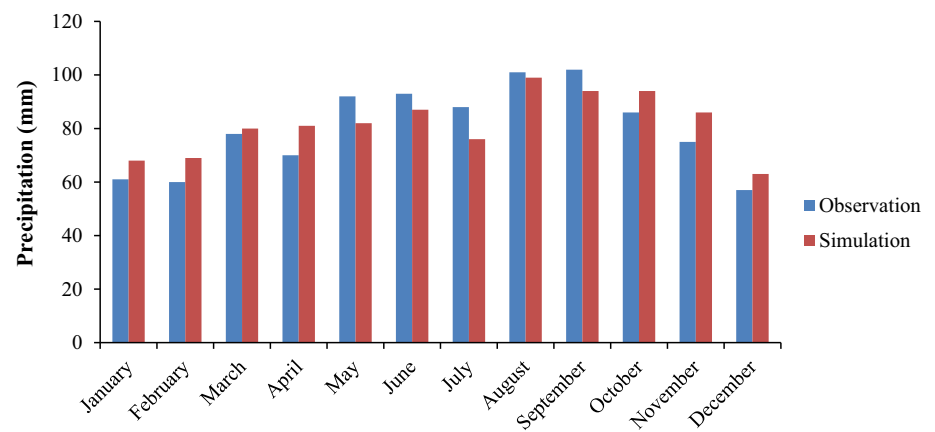


**Table 2** Mean annual precipitations under LARS-WG scenarios (mm)

Station	1991–2010	A2 2011–2030	B1 2031–2050	2011–2030	2031–2050
Darzi Kola	618	690	594	703	630
Kaleh	686	708	676	733	699
Rig Cheshmeh	752	1074	1024	1105	1043
Sangdeh	846	897	829	923	851
Shirgah	1045	1044	954	1074	991
Talar	987	1112	1045	1078	1061
Mean	822	921	854	936	879

that of basis period and September and December had the maximum and minimum rainfall amount.

The result of climate change scenarios at SDSM-DC model showed by applying the first scenario (10% increase in precipitation) in the first period of stimulated future climate, rainfall value will increase by 13% when compared to basis period and also mean rainfall will increase by 126 mm in study area. In the second scenario (10% reduction in precipitation), the mean rainfall will reduce by

53 mm, and finally, in the third scenario (unchanged precipitation), the mean rainfall will increase by 48 mm. The results of first and second simulated periods indicate if the 10% increases in precipitation or unchanged precipitation exist, for both of the simulated scenarios, the amount of annual rainfall will be more than that of the basis period. However, if 10% reduction in precipitation exists, the amount of annual rainfall will reduce in both the simulated scenarios when compared to the basis period (Table 3).



**Fig. 5** Comparison in the mean of rainfall under the LARS-WG scenarios in basis and simulated period

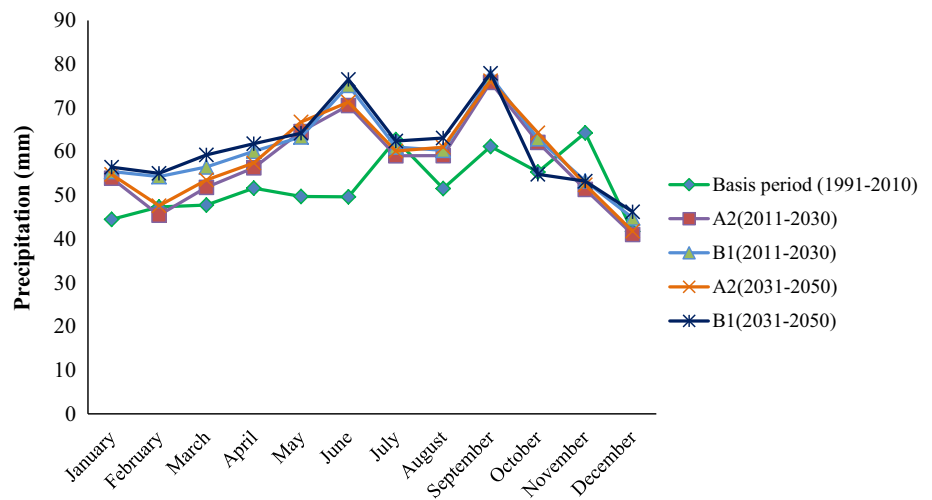


**Table 3** Mean annual precipitations under SDSM-DC scenarios (mm)

Station	1991–2010	10% increase in precipitation		Unchanged precipitation		10% decrease in precipitation	
		2011–2030	2031–2050	2011–2030	2031–2050	2011–2030	2031–2050
Darzi Kola	618	738	627	624	620	604	593
Kaleh	686	760	722	707	694	615	599
Rig Cheshmeh	752	825	783	799	782	712	684
Sangdeh	846	980	905	900	873	802	763
Shirgah	1045	1087	1076	998	965	890	874
Talar	987	1282	1241	1177	1169	972	955
Mean	822	945	892	867	850	769	745

**Annual soil loss in the basis period**

Model input parameters were derived using remote sensing data and field survey and integrated in GIS environment to compute average annual soil loss and assess the soil erosion risk in Kasilian watershed. The five-parameter layers were all converted into a grid with 30 × 30 m cells in a uniform coordinate system. The GIS input layers were then multiplied, as described by the RUSLE, to estimate annual soil loss on a pixel-by-pixel basis, and the spatial distribution of the soil erosion in the study area was obtained.

The input maps of *R* factor of the whole watershed were interpolated employing a spline interpolation through GIS (Fig. 6). From Fig. 6, it can be seen that erosivity values are reduced from northwest to southeast depending on precipitation characteristics. The minimum and maximum *R* value for the study area was 179 and 272 MJ mm ha<sup>-1</sup> h<sup>-1</sup> year<sup>-1</sup> in basis period. *K* values ranged from 0.32 to 0.44, and the map of *K* values was generated to illustrate spatial distribution of erodibility

(Fig. 6). A topography map with a spatial resolution of 30 m was used to develop a map of the slope length and slope steepness factor (*LS*) by using (8) and (9). The highest *LS* value for the Kasilian watershed was calculated as 54.235. *C* value is provided using land use map 2011 (Fig. 6), and the maximum and minimum amounts of *C* value are for rangeland and forest, respectively. *P* factor values are assumed as 1 for the watershed, because only a very small area has conservation practices. As seen in Fig. 6, average annual soil loss is between 0 and 1022 tons h<sup>-1</sup> year<sup>-1</sup>.

In line with the studies, the results of rain erosion intensity showed that in areas where rainfall erosivity was more than other points, the risk of soil erosion in the area has increased equally. Rain erosion rates are reduced from the northwest to the southeast of watershed, which is related to the rainfall reduction as well as rainfall uneven spatial distribution in the watershed. The increase in slope length led to increased power water flow and transmission of the erosion force in higher levels of soil and the

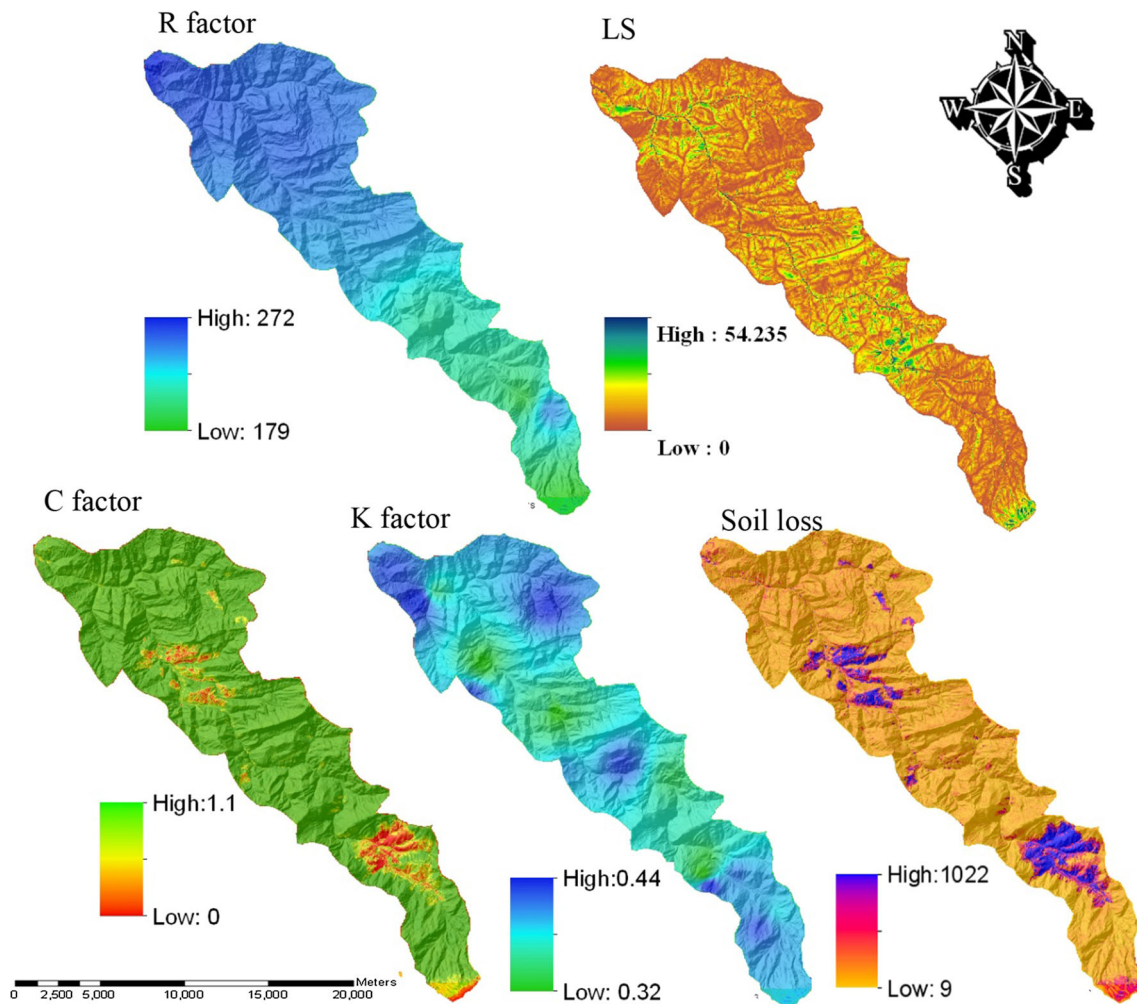


**Fig. 6** Input of RUSLE model in study area

amount of erosion is increased (Ranzi et al. 2012). The results are in agreement with the results of many studies such as Prasannakumar et al. (2012), Ranzi et al. (2012) based on the direct role of slope length to increase the erosion rate. The results showed that vegetation cover is the most important obstacle against erosion and the increased erosion through converting each land use into residential representing the effects caused by human intervention. Soil erodibility map showed that in the areas with loam texture, the erosion rate was higher than the other areas and the areas with clay loam texture have lower erosion rate. In general, there is a close relationship between the aggregate stability and erodibility factor, so that the erosion resistance increases by decreasing the diameter (Giglio et al. 2014; Stanchi et al. 2015). Therefore, by increasing the clay content, the adhesive force

between soil particles is enhanced, permeability and hydraulic conductivity of the soil are decreased, and the shear force is increased to carry the soil. On the other hand, in some areas of watershed where bare soils faced with severe weathering, the  $K$  value was higher than other areas. The final map of soil erosion risk in the basis period showed that most of the surfaces of the study area were in poor and low erosion level because many parts of the Kasilian watershed were in forest areas with appropriate vegetation cover. The vicinity of villages and pastures with fields for dry farming that were later abandoned, along with land use changes, especially from forest to residential, as well as conversion of dense forests into semi-dense forests and forest into pasture, were at high risk and very high erosion level. The weighing map of soil loss rate shows that the soil loss rate in Kasilian

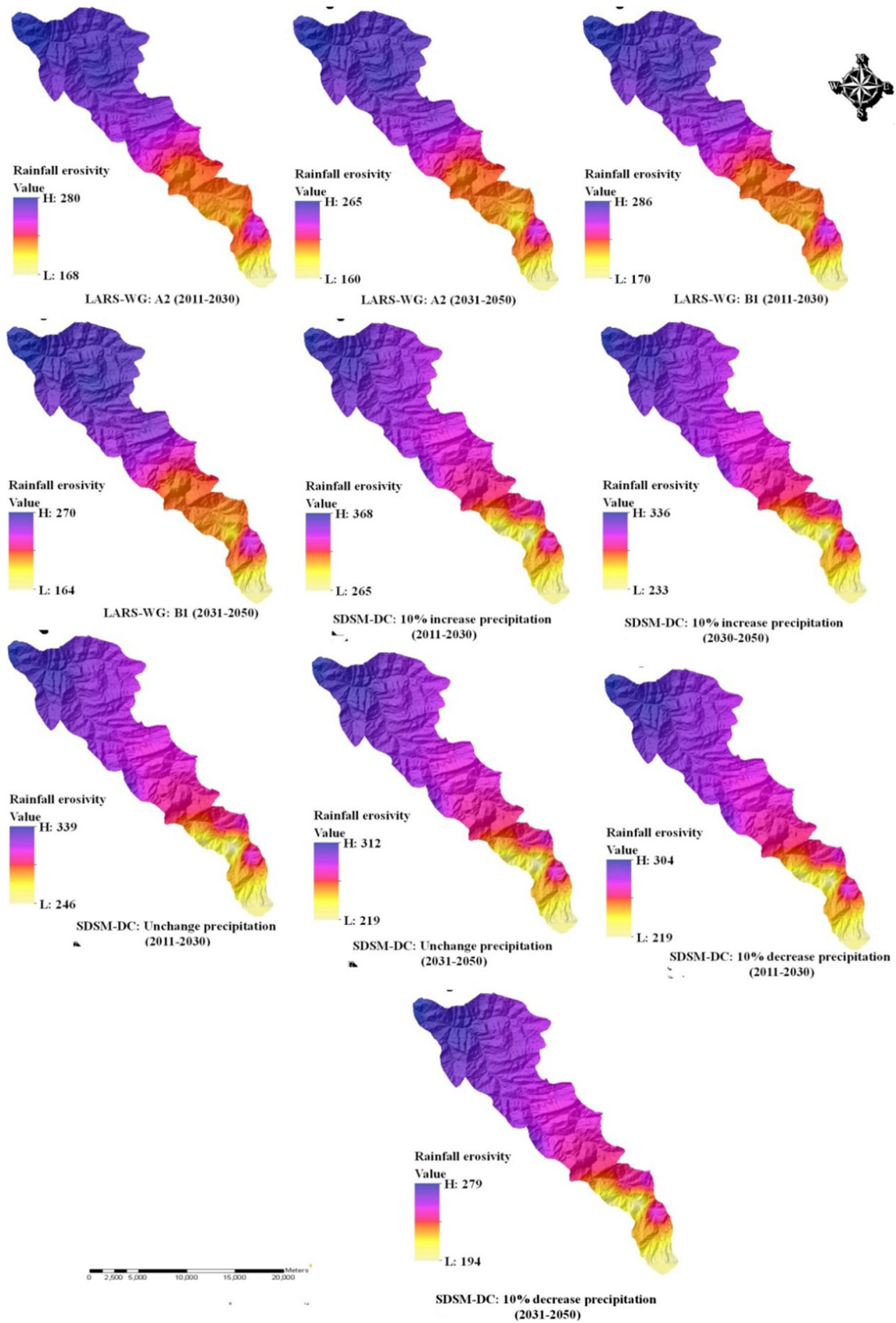


Fig. 7 Rainfall erosivity map in future period

watershed is between 0 and 1022 tons  $\text{ha}^{-1}$  year $^{-1}$  in which the highest soil loss rate is in the pastures in vicinity of villages as well as the areas with poor vegetation cover.

### Annual soil loss in the future period

To simulate soil erosion in future period, all climate change scenarios were applied on the rainfall erosivity. Thereafter, rainfall erosivity zonation maps were prepared for all future climate scenarios (Fig. 7). The results showed that the 10% increase in rainfall scenario in the SDSM-DC model has the most erosivity between all the scenarios and in all of the rainfall erosivity maps, and erosivity value in future period has increased in comparison to basis period that these results are in line with the results of studies Zhang et al. (2009), Litschert et al. (2014) and Plangoen and Babel (2014) in rainfall erosivity increase. In fact, the results showed that changes in rainfall erosivity index are totally related to rise and fall of annual rainfall value. In addition, results indicated that between different levels of rainfall erosivity, there will be increase in rainfall erosivity in terms of type of scenario during the future period. So that with 10% increase in rainfall trend, rainfall erosivity value will increase by 35% and even if rainfall trends decrease by 10%, the erosivity will also increase by 11%, too. On the other hand, if the trend of precipitations does not change, rainfall erosivity will increase by 24% in the study area, and thus, increase in rainfall erosivity trend will be unavoidable for future period. Zhang et al. (2009) in China with A2 and B1 scenarios have estimated 20% increase in rainfall erosivity in three periods of 2020, 2050 and 2080. Also, Segura et al. (2014) in the USA and Plangoen and Babel (2014) in Thailand have predicted 11 and 14% increase in rainfall erosivity in future. Spatial changes in rainfall erosivity showed that rainfall erosivity boundary will change in future years and will move toward high areas. Nearing et al. (2005) and Diodato and Bellocchi (2007) have confirmed the trend of increase in rainfall erosivity in the high areas. Orographic rainfalls and changes due to population increase and land use change are among the main reasons for rainfall changes that directly affect the rainfall erosivity (Bonacina 1945).

In the next step, by multiplying all the simulated rainfall erosivity maps in the inputs of RUSLE model, soil loss value was obtained for 2011–2030 and 2031–2050 periods.

**Table 4** Type of soil erosion scenario in study area

Type of soil erosion scenario	Scenario cod
A2 scenario for 2011–2030	1
B1 scenario for 2011–2030	2
A2 scenario for 2031–2050	3
B1 scenario for 2031–2050	4
10% increase in rainfall for 2011–2030	5
10% increase in rainfall for 2031–2050	6
Unchanged of rainfall for 2011–2030	7
Unchanged of rainfall for 2031–2050	8
10% decrease in rainfall for 2011–2030	9
10% decrease in rainfall for 2031–2050	10

Furthermore, soil erosion scenarios were calculated based on ten climate change scenarios in Table 4.

According to the maximum and minimum erosion condition in erosion hazard map (Fig. 8), the mean of each erosion scenario with the mean of erosion in basis period is shown in Fig. 9. As it can be seen in this figure, 10% increase in rainfall scenario has the most significant soil loss value in the all of climate change scenarios in 2030. Also, soil erosion under the influence of climate change scenarios in SDSM-DC model is much more than LARS-WG model. The results showed that soil erosion value in basis period was lower than all scenarios of climate change for 2030 and 2050. So that, according to scenarios 7 and 8, if rainfall changes trend is constant, soil erosion value will increase in future years in comparison to basis period, and therefore, the increase in soil erosion will be definite in the future. Bosco et al. (2009) and Plangoen and Babel (2014) also estimated the increase in erosion in the coming decades. Given this potential for climate change to increase soil erosion rates and its impacts, modeling future erosion rates is a crucial step in assessing the potential future of agricultural and environmental problems that may accompany increasing erosion rates.

### Conclusion

Soil loss was predicted to increase from the period of 1991–2010 to 2011–2050 according to a series of simulations utilizing the RUSLE erosion model with LARS-WG and SDSM-DC downscaling models. The climate changes have had an important impact on the rainfall erosivity.

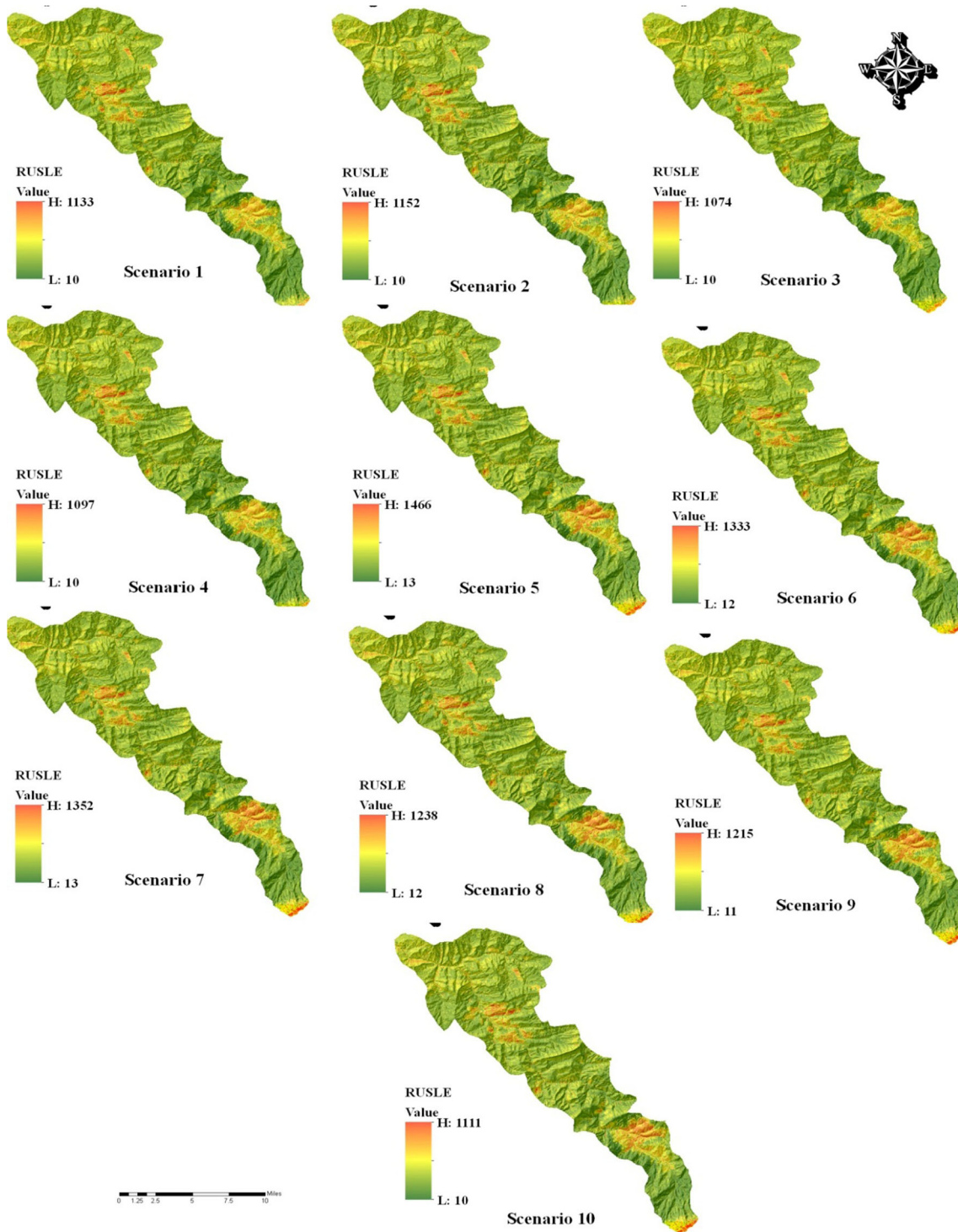
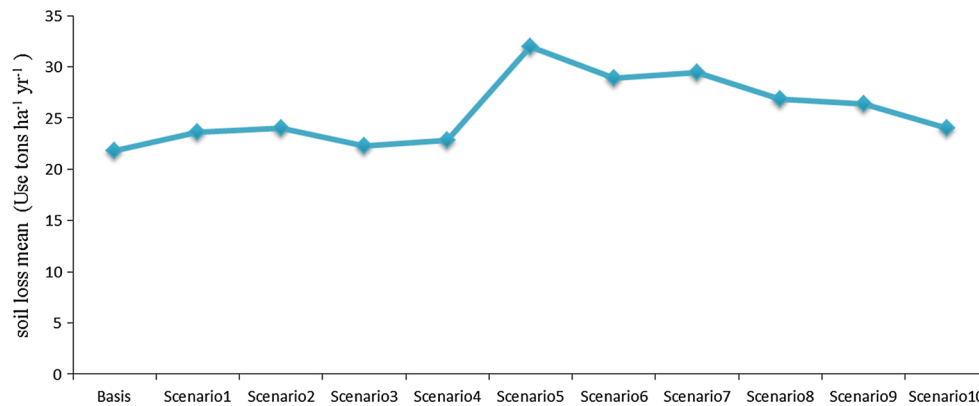


Fig. 8 Simulation of soil erosion map under the influence of climate change scenarios



**Fig. 9** Mean of soil erosion under climate change scenarios

With every change in climate scenarios, change in rainfall erosivity can also be expected. With a 1% increase in rainfall erosivity, soil erosion value will increase from 0.8 to 1%. Therefore, the results have demonstrated that all soil erosion scenarios were more than soil erosion of the basis period. Even if there is no change in rainfall trend until 2030 and 2051, soil erosion will increase by 35 and 23%, respectively, and thus, increase in soil erosion will be definite in future.

## References

- Alkharabsheh MM, Alexandridis TK, Bilas G, Misopolinos N, Silleos N (2013) Impact of land cover change on soil erosion hazard in northern Jordan using remote sensing and GIS. *Proced Environ Sci* 19:912–921
- Ashraf B, Mousavi Baygi M, Kamali GA, Davari K (2010) Prediction of water requirement of sugar beet during 2011–2030 by using simulated weather data with LARS-WG downscaling model. *J Water Soil* 25(5):1184–1196 (**In Persian**)
- Auerswald K, Fiener P, Martin W, Elhaus D (2014) Use and misuse of the K factor equation in soil erosion modeling: an alternative equation for determining USLE nomograph soil erodibility values. *Catena* 118:220–225
- Bonacina LC (1945) Orographic rainfall and its place in the hydrology of the globe. *Q J R Meteorol Soc* 71:41–55
- Bosco C, Rusco E, Montanarella L, Panagos P (2009) Soil erosion in the Alpine area: risk assessment and climate change. *Stud Trent Sci Nat* 85:117–123
- Chu JT, Xia J, Xu CY (2008) Suitability analysis of SDSM model in the Haihe River basin. *Resour Sci* 30(12):1825–1832
- Dibike YB, Coulibaly P (2005) Hydrologic impact of climate change in the Saguenay watershed: comparison of downscaling methods and hydrologic models. *J Hydrol* 307(1–4):145–163
- Diodato N, Bellocchi G (2007) Estimating monthly (R) USLE climate input in a Mediterranean region using limited data. *J Hydrol* 345(3–4):224–236
- Favis-Mortlock DT, Guerra AJT (1999) The implications of general circulation model estimates of rainfall for future erosion: a case study from Brazil. *Catena* 37(3–4):329–354
- Giglo BF, Arami A, Akhzari D (2014) Assessing the role of some soil properties on aggregate stability using path analysis (case study: silty-clay-loam and clay-loam soil from gully lands in North west of Iran). *Ecopersia* 2(2):513–523
- Hashmi MZ, Shamseldin AY, Melville B (2009) Statistical downscaling of precipitation: state-of-the-art and application of Bayesian multimodel approach for uncertainty assessment. *Hydrol Earth Syst Sci* 6:6535–6579
- Hassan Z, Shamsudin S, Harun S (2014) Application of SDSM and LARS-WG for simulating and downscaling of rainfall and temperature. *Theor Appl Climatol* 116(1):243–257
- Hessami M, Gachon P, Quarda T, St-Hilaire A (2008) Automated regression based statistical downscaling tool. *Environ Model Softw* 23:813–834
- Imeson AC, Lavee H (1998) Soil erosion and climate change: the transect approach and the influence of scale. *Geomorphology* 23(2–4):219–227
- IPCC (2001) Climate change: the scientific basis. In: Houghton JT, Ding Y, Griggs DJ, Noguer M, van der Linden PJ, Dai X, Maskell K, Johnson CA (eds) *Contribution of Working Group I to the Third Assessment Report of the Intergovernmental Panel on Climate Change*. Cambridge University Press, Cambridge
- Khan MS, Coulibaly P, Dibike Y (2006) Uncertainty analysis of statistical downscaling methods. *J Hydrol* 319:357–382
- Lal R (1998) Soil erosion impact on agronomic productivity and environment quality: critical reviews. *Plant Sci* 17(4):319–464
- Lal R (2001) Soil degradation by erosion. *Land Degrad Dev* 12(6):519–539
- Litschert SE, Theobald DM, Brown TC (2014) Effects of climate change and wildfire on soil loss in the Southern Rockies Ecoregion. *Catena* 118:206–219
- Liu LL, Liu ZF, Xu ZX (2008) Trends of climate change for the upper-middle reaches of the Yellow River in the 21st century. *Adv Clim Change Res* 4(3):167–172
- Liu L, Liu Z, Ren X, Fischer T, Xu Y (2011) Hydrological impacts of climate change in the Yellow River Basin for the 21st century using hydrological model and statistical downscaling model. *Quat Int* 244(2):211–220
- Maeda E, Pellikka P, Siljander M, Clark B (2010) Potential impacts of agricultural expansion and climate change on soil erosion in the. *Geomorphology* 123:279–289
- Meusbürger K, Steel A, Panagos P, Montanarella L, Alewell C (2012) Spatial and temporal variability of rainfall erosivity factor for Switzerland. *Hydrol Earth Syst Sci* 16(1):167–177
- Moore ID, Burch GJ (1986) Physical basis of the length-slope factor in the universal soil loss equation. *Soil Sci Soc Am J* 50:1294–1298
- Mullan D (2013) Soil erosion under the impacts of future climate change: assessing the statistical significance of future changes and the potential on-site and off-site problems. *Catena* 109:234–246

- Mullan D, Mortlock DF, Fealy R (2012) Addressing key limitations associated with modelling soil erosion under the impacts of future climate change. *Agric For Meteorol* 156:18–30
- Nearing AM (2001) Potential changes in rainfall erosivity in the U.S. with climate change during the 21st century. *J Soil Water Conserv* 56(3):229–232
- Nearing MA, Jetten V, Baffaut C (2005) Modeling response of soil erosion and runoff to changes in precipitation and cover. *Catena* 61(2–3):131–154
- Nearing MA, Unkrich CL, Goodrich DC, Nichols MH, Keefer TO (2015) Temporal and elevation trends in rainfall erosivity on a 149 km<sup>2</sup> watershed in a semi-arid region of the American southwest. *Int Soc Water Conserv Res* 3(2):77–85
- Oneal MR, Nearing MA, Vining RC, Southworth J, Pfeifer RA (2005) Climate change impacts on soil erosion in Midwest United States with changes in crop management. *Catena* 61(2–3):165–184
- Park S, Oh C, Jeon S, Jung H, Choi C (2011) Soil erosion risk in Korean watersheds, assessed using the revised universal soil loss equation. *J Hydrol* 399(3–4):263–273
- Pimentel D (2006) Soil erosion: a food and environmental threat. *Environ Dev Sustain* 8:119–137
- Plangoen P, Babel M (2014) Projected rainfall erosivity changes under future climate in the Upper Nan Watershed, Thailand. *J Earth Sci Clim Change* 5(10):1–7
- Portenga EW, Bierman PR (2011) Understanding Earth's eroding surface with 10 Be. *GSA Today* 21:4–10
- Pradeep GS, Krishnan MV, Vijith H (2015) Identification of critical soil erosion prone areas and annual average soil loss in an upland agricultural watershed of Western Ghats, using analytical hierarchy process (AHP) and RUSLE techniques. *Arab J Geosci* 8(6):3697–3711
- Prasannakumar V, Vijith H, Abinod S, Geetha N (2012) Estimation of soil erosion risk within a small mountainous sub-watershed in Kerala, India, using Revised Universal Soil Loss Equation (RUSLE) and geoinformation technology. *Geosci Front* 3(2):209–215
- Pruski FF, Nearing MA (2002a) Climate-induced changes in erosion during the 21st century for eight U.S. locations. *Water Resour Res* 38(12):34–44
- Pruski FF, Nearing MA (2002b) Runoff and soil loss responses to changes in precipitation: a computer simulation study. *J Soil Water Conserv* 57(1):7–16
- Ranzi R, Le TH, Rulli MC (2012) A RUSLE approach to model suspended sediment load in the Lo river (Vietnam): effects of reservoirs and land use changes. *J Hydrol* 422–423:17–29
- Renard KG, Freimund JR (1994) Using monthly precipitation data to estimate the R-factor in the revised USLE. *J Hydrol* 157(1–4):287–306
- Renard KG, Foster GR, Weesies GA, McCool DK, Yoder DC (1997) Predicting soil erosion by water: a guide to conservation planning with the revised Universal Soil Loss Equation (RUSLE). US Department of Agriculture, Agriculture Handbook, No. 573
- Segura C, Sun G, McNulty S, Zhang Y (2014) Potential impacts of climate change on soil erosion vulnerability across the conterminous United States. *J Soil Water Conserv* 69:171–181
- Semenov MA, Donatelli M, Stratonovitch P, Chatzidaki E, Baruth B (2010) ELPIS: a dataset of local-scale daily climate scenarios for Europe. *Clim Res* 44:3–15
- Serpa D, Nunes JP, Santos J, Sampaio E, Jacinto R, Veiga S, Lima JC, Moreira M, Corte-Real J, Keizer JJ, Abrantes N (2015) Impacts of climate and land use changes on the hydrological and erosion processes of two contrasting Mediterranean catchments. *Sci Total Environ* 538:64–77
- Shiono T, Ogawa S, Miyamoto T, Kameyama K (2013) Expected impacts of climate change on rainfall erosivity of farmlands in Japan. *Ecol Eng* 61:678–689
- Simonneau V, Cheggour A, Deschamps C, Mouillot F, Cerdan O, Bissonnais Y (2015) Land use and climate change effects on soil erosion in a semi-arid mountainous watershed (High Atlas, Morocco). *J Arid Environ* 122:64–75
- Stanchi S, Falsone G, Bonifacio E (2015) Soil aggregation, erodibility, and erosion rates in mountain soils (NW Alps, Italy). *Solid Earth* 6:403–414
- Vrieling A, Hoedjes JB, Velde MV (2014) Towards large-scale monitoring of soil erosion in Africa: accounting for the dynamics of rainfall erosivity. *Glob Planet Change* 115:33–43
- Ward PJ, Balen RT, Verstraeten G, Renssen H, Vandenberghe J (2009) The impact of land use and climate change on late Holocene and future suspended sediment yield of the Meuse catchment. *Geomorphology* 103(3):389–400
- Wardle DA, Bardgett RD, Klironomos JN, Setälä H, van der Putten WH, Wall DH (2004) Ecological linkages between aboveground and belowground biota. *Science* 304:1634–1637
- Wilby RL, Harris I (2006) A frame work for assessing uncertainties in climate change impacts: low flow scenarios for the River Thames, UK. *Water Res*. doi:10.1029/2005WR004065
- Wilby RL, Dawson CW, Barrow EM (2002) SDSM—a decision support tool for the assessment of regional climate change impacts. *Environ Model Softw* 17(2):147–159
- Wilby RL, Dawson CW, Murphy C, O'Connor P, Hawkins E (2014) The Statistical DownScaling Model-Decision Centric (SDSM-DC): conceptual basis and applications. *Clim Res* 61:259–276
- Wischmeier WH, Smith DD (1978) Predicting rainfall erosion losses: A guide to conservation planning. US Department of Agriculture, Agriculture Handbook, No. 573
- Wischmeier WH, Johnson CB, Cross BV (1971) A soil erodibility nomograph for farmland and construction sites. *J Soil Water Conserv* 26:189–193
- Xu ZX, Zhao FF, Li JY (2009) Response of streamflow to climate change in the headwater catchment of the Yellow River basin. *Quat Int* 208:62–75
- Zhang XC, Liu WZ, Li Z, Zheng FL (2009) Simulating site-specific impacts of climate change on soil erosion and surface hydrology in southern Loess Plateau of China. *Catena* 79(3):237–242